

Article

# Desorption Kinetics and Mechanisms of CO<sub>2</sub> on Amine-Based Mesoporous Silica Materials

Yang Teng, Zhilin Liu, Gang Xu and Kai Zhang \*

Beijing Key Laboratory of Emission Surveillance and Control for Thermal Power Generation, North China Electric Power University, Beijing 102206, China; tengyang@ncepu.edu.cn (Y.T.); zhilinlau@ncepu.edu.cn (Z.L.); 50201637@ncepu.edu.cn (G.X.)

\* Correspondence: kzhang@ncepu.edu.cn; Tel.: +86-10-6177-2413

Academic Editor: Fernando Rubiera González

Received: 15 November 2016; Accepted: 5 January 2017; Published: 18 January 2017

**Abstract:** Tetraethylenepentamine (TEPA)-based mesoporous MCM-41 is used as the adsorbent to determine the CO<sub>2</sub> desorption kinetics of amine-modified materials after adsorption. The experimental data of CO<sub>2</sub> desorption as a function of time are derived by zero-length column at different temperatures (35, 50, and 70 °C) and analyzed by Avrami's fractional-order kinetic model. A new method is used to distinguish the physical desorption and chemical desorption performance of surface-modified mesoporous MCM-41. The activation energy  $E_a$  of CO<sub>2</sub> physical desorption and chemical desorption calculated from Arrhenius equation are 15.86 kJ/mol and 57.15 kJ/mol, respectively. Furthermore, intraparticle diffusion and Boyd's film models are selected to investigate the mechanism of CO<sub>2</sub> desorption from MCM-41 and surface-modified MCM-41. For MCM-41, there are three rate-limiting steps during the desorption process. Film diffusion is more prominent for the CO<sub>2</sub> desorption rates at low temperatures, and pore diffusion mainly governs the rate-limiting process under higher temperatures. Besides the surface reaction, the desorption process contains four rate-limiting steps on surface-modified MCM-41.

**Keywords:** amine modified MCM-41; desorption kinetics; zero length column; Avrami's fractional model; intraparticle diffusion; film diffusion

## 1. Introduction

CO<sub>2</sub> capture and sequestration (CCS) could reduce greenhouse gas emissions and enable low-carbon electricity generation from power plants [1]. In order to reduce the overall cost and increase the possibility of practical application of CCS, solid adsorption becomes a competitive and viable method for CO<sub>2</sub> removal, and most of the researches focus on the development of adsorbents with high CO<sub>2</sub> capacity and efficiency [2–5]. Mesoporous MCM-41 has been extensively reported as an adsorbent for CO<sub>2</sub> adsorption due to its mature synthesis technique and the possibility of surface modification. Amine-based mesoporous materials are promising in terms of adsorption capacity, selectivity, and stability. It is attractive to study the adsorption behavior for subsequent simulation and application. Physical adsorption tends to be minor under high temperatures, which is a drawback for adsorbing CO<sub>2</sub> from flue gases. In contrast, chemical adsorption shows a higher adsorption capacity and can operate under high temperatures due to the chemical reaction between amine groups and CO<sub>2</sub> [6,7]. Some researchers have reported that tetraethylenepentamine (TEPA)-based MCM-41 showed superior adsorption performance [8–10]. As a result, in this work, MCM-41 and TEPA-modified MCM-41 were chosen as the adsorbent. Previous work has focused on the total capacity as a criterion of effectiveness, but has rarely considered adsorption kinetics and mechanism.

The adsorption kinetics has been studied by many researchers, but there is still lack of study of desorption kinetics. However, the time dependency of desorption processes is crucial to obtain the

kinetic parameters and to design the CO<sub>2</sub> capture reactors. There are significant energy ramifications when altering the adsorbents' properties, especially the adsorption heat. Hereafter, the effect of adsorbent properties and process parameters on the total energy penalty is examined in this work, which could help to determine the size of the system and the energy penalty of the process. The CO<sub>2</sub> desorption kinetics in amine-modified mesoporous MCM-41 are controlled both by pore structures and by chemical-functionalized groups [11]. A new method was used to distinguish the percentage of chemical and physical desorption. In order to gain further insights into the CO<sub>2</sub> adsorption on MCM-41 and MCM-41-TEPA, Avrami's model was applied to calculate the desorption heat needed to unbind the CO<sub>2</sub> molecules onto adsorbent, with the aim of building a strong basis for simulation. This work was designed to interpret the desorption kinetics of amine-modified mesoporous MCM-41.

Since introduced by Eic and Ruthven [12] for measuring the intracrystalline diffusivities in strongly adsorbed species, the zero-length column (ZLC) technique has been used extensively to study the adsorption performance in porous adsorbents due to its apparent simplicity [13,14]. ZLC was used to conduct the adsorption experiments herein described. The external mass transfer resistances and heat effects are minimized by the high flow-to-particle-mass ratio and the large thermal mass of the column in which a small amount of sample is packed [15].

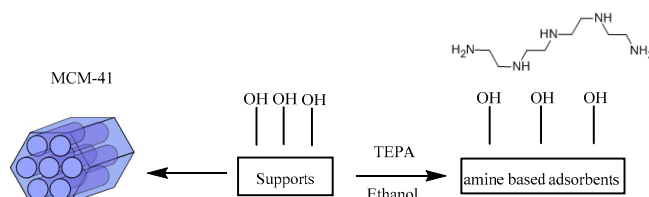
The adsorption mechanism in porous materials has been investigated in terms of both a pore-filling process and a surface adsorption. Martinez et al. [16] studied the adsorption mechanism of CO<sub>2</sub> on activated anthracite and found that the adsorption was a pore-filling process in narrow micropores. Adsorption in wide pores dominated throughout surface adsorption. However, few works interpret the adsorption mechanism in mesoporous adsorbents, not to mention the desorption mechanism. Bacsik et al. [17] used (3-aminopropyl) triethoxysilane- or (3-aminopropyl) methyl-diethoxysilane-modified AMS-6 and MCM-48 as the adsorbents. IR spectra was performed to study the adsorption mechanism and concluded ammonium carbamate ion pairs and carbamic acid formed rapidly. The desorption mechanism of CO<sub>2</sub> is still not clear, which is important to calculate energy requirements for regeneration and design of the CO<sub>2</sub> capture reactors.

As mentioned earlier, the desorption performance is essential for CO<sub>2</sub> separation technology. Therefore, it is a key point to understand the desorption kinetics and mechanism for the development of this technology. This work also gives a better understanding of chemical and physical CO<sub>2</sub> desorption on amine modified mesoporous materials.

## 2. Experimental

### 2.1. Materials Preparation

MCM-41 was used as the support in this work, as mentioned earlier. TEPA-based MCM-41 was synthesized by the procedure as reported elsewhere [8,18]. The modified MCM-41 with TEPA loading of 40 wt % had the highest adsorption capacity compared with other loadings. In a typical batch, 0.2 g TEPA was added into 10 mL of dry ethanol. After dissolution, 0.5 g of MCM-41 was added under stirring conditions. Then, it was statically kept at room temperature for 12 h. The resultant precipitate was dried at 100 °C for 16 h. The process is shown in Scheme 1. The obtained sample is denoted as MCM-41-TEPA in the results.



**Scheme 1.** Preparation of tetraethylenepentamine (TEPA)-impregnated MCM-41 adsorbents by impregnation.

## 2.2. Materials Characterization

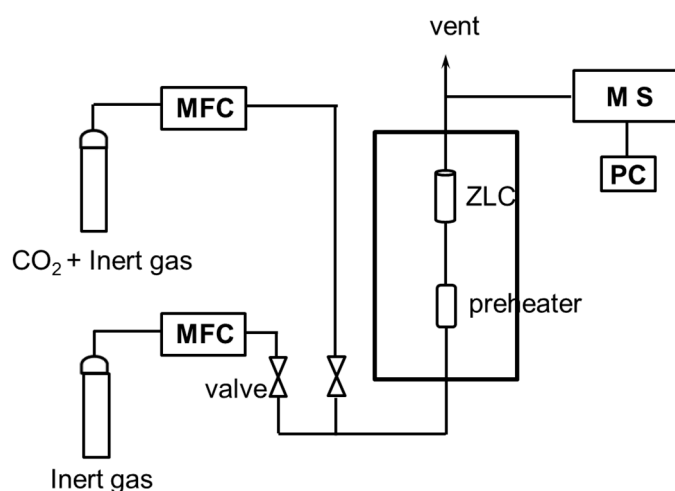
The crystal structure of original MCM-41 and amine-based MCM-41 was characterized by X-ray diffraction (XRD) on D8 ADVANCE (Bruker, Karlsruhe, Germany) diffractometer operating at 40 kV and 30 mA with Cu-K $\alpha$  radiation (0.1541 nm). The XRD patterns were taken in the  $2\theta$  range of  $1.3^\circ$ – $10^\circ$  at a scan speed of  $0.5^\circ \text{ min}^{-1}$ .

Pore diameter, volume, and surface area of samples synthesized were evaluated via N<sub>2</sub> physical adsorption analysis through ASAP2020 (Micromeritics, Norcross, GA, USA) automatic adsorption system. Each sample was degassed at 350 °C and 1.33 Pa under N<sub>2</sub> flow for 5 h prior to measurement. The N<sub>2</sub> adsorption data was recorded at the liquid N<sub>2</sub> temperature ( $-196^\circ \text{C}$ ). The surface area and the pore size distribution were calculated by the Brunauer–Emmett–Teller (BET) and Barrett–Joyner–Halenda (BJH) equations, and the total pore volume was estimated from the amount of adsorbed N<sub>2</sub> at the partial pressure  $P/P_0 = 0.99$ .

Elemental analysis was carried out by using the vario MACRO cube elemental analyzer (Elementar, Munchen, Germany) to determine C, H, and N content in the samples. Infrared spectra of MCM-41 and amine-based MCM-41 were recorded in the 4000–450  $\text{cm}^{-1}$  region using Spectrum100 Fourier-transform infrared (FT-IR) (PerkinElmer, Waltham, MA, USA).

## 2.3. CO<sub>2</sub> Desorption Process

Scheme 2 illustrates the simplified schematic diagram of the ZLC system used for the experiment. The ZLC column was packed with MCM-41 or MCM-41-TEPA with nonadsorbing rock wool. The wool was used to avoid the gas bypass. The adsorbent was thermally regenerated under pure helium at 100 °C for 1 h of 2 mL/min. Then, the oven temperature was reduced to 35 °C, 50 °C, and 70 °C to begin the experiments. The feed gas mixture was prepared inside a dosing oven, and drying columns were used to ensure that the gases were dry. In a ZLC experiment, the sample is first exposed to 10% CO<sub>2</sub> and 90% He to reach the adsorption equilibrium, and then the gas is switched to pure helium at the same flow rate. DycorAmetekBenchtopquadrupole mass spectrometer (MS) was used to conveniently detect the change of outlet gas concentration. A computer monitored the signal produced by MS.



**Scheme 2.** Schematic diagram of the zero-length column (ZLC) system.

## 3. Results and Discussion

### 3.1. Material Characterization and Desorption Isotherms

Table 1 summarizes the characteristics and elemental analysis of MCM-41 and MCM-41-TEPA, as calculated from N<sub>2</sub> adsorption/desorption isotherm. After impregnation of TEPA on MCM-41,

the mesoporous structure of MCM-41 is well maintained, although the surface area decreased. Elemental analysis reveals that TEPA was successfully impregnated onto MCM-41.

**Table 1.** The characteristics and the operation condition of MCM-41 and MCM-41-TEPA.

	MCM-41		MCM-41-TEPA				
Surface area (m <sup>2</sup> /g)	865		364				
Pore volume (cm <sup>3</sup> /g)	1.00		0.4				
Pore size (nm)	4.64		3.62				
Samples	Elemental Analysis				Desorption Capacity (mmol/g)		
	C%	H%	S%	N%	35 °C	50 °C	70 °C
MCM-41	2.01	0.56	0.07	0.26	0.15	0.10	0.08
MCM-41-TEPA	19.32	4.81	0.10	10.22	1.35	1.10	0.80

Figure 1 shows the ZLC response curves plotted as  $c/c_0$  vs.  $t$ . Clearly, under the same conditions, the desorption capacity of MCM-41 and MCM-41-TEPA under different temperatures are diverse. MCM-41-TEPA yields desorption capacity superior to MCM-41. The total CO<sub>2</sub> capacity is the integral of the curve (i.e., the area under the curve). Through calculating the area, the desorption capacity could be obtained.

The common assumption in the ZLC experiments is that the flow rate of the carrier gas keeps constant. The outlet flow rate can be approximated by Equation (1):

$$(Fy)_{out} = \frac{F_{in}}{1-y} y_{out} \quad (1)$$

where  $y$  is the mole fraction of the adsorbing species and  $F$  is the volumetric flow rate (mL/min), which follows as Equation (2):

$$\frac{c}{c_0} = \frac{y}{y_0} \quad (2)$$

The mass balance is:

$$V_S \frac{d\bar{q}}{dt} + V_g c \frac{dy}{dt} + F_{in} c \frac{y}{1-y} = 0 \quad (3)$$

where  $V_g$  represents the gas volume (m<sup>3</sup>/g),  $V_S$  is the solid volume,  $\bar{q}$  is the average adsorbed phase concentration (mmol/g), and  $c$  is the sorbate concentration (mmol/g) in the gas phase. Here, the gas phase concentration is measured. This equation can be integrated to obtain the complete isotherm as Equation (4):

$$q^* = \int_0^\infty \frac{FCy}{V_S} dt - \int_0^t \frac{FCy}{V_S} dt - \frac{V_g C}{V_S} y \quad (4)$$

The total effluent flow rate,  $F$ , is not constant due to the desorption of the adsorbate. So, the above equation can be rewritten as Equation (5), referring the flow rate ( $F_C$ ) of the purge gas, which is approximately the constant:

$$q^* = \frac{F_C}{V_S} \int_0^\infty \frac{Cy}{1-y} dt - \frac{F_C}{V_S} \int_0^t \frac{Cy}{1-y} dt - \frac{V_g C}{V_S} y \quad (5)$$

where  $C$  is the total concentration, which is calculated from the ideal gas law,  $C = P/(RT)$ . Integration of Equation (5) allows us to calculate the total capacity. For strongly adsorbed components, the exponential tail can be approximated by an analytical function. This method could determine the integral more accurately [19]. The results are depicted in Table 1. The capacities of MCM-41-TEPA under 35, 50, and 70°C are superior to MCM-41.

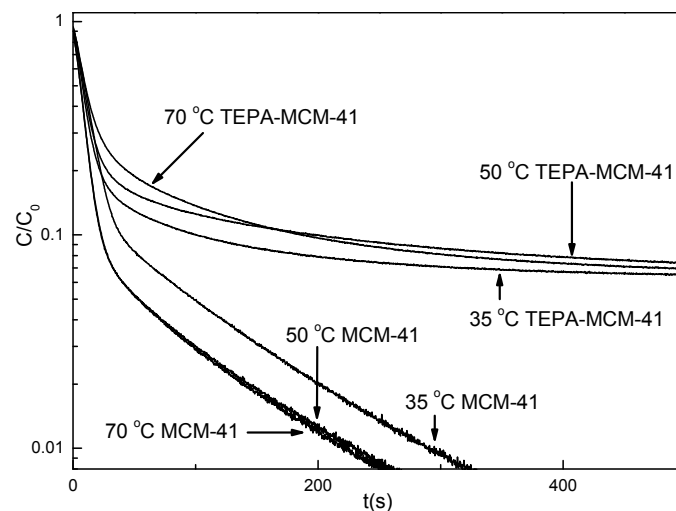


Figure 1. Desorption curves of MCM-41 and MCM-41-TEPA.

### 3.2. Desorption Kinetics

Fast adsorption kinetics is one of the most important properties when evaluating a good adsorbent [20–23]. Currently, a lot of kinetic models are proposed to describe the experimental data. For example, Langmuir model [24,25], Langmuir–Freundlich model [26,27], pseudo-first-order [28], pseudo-second-order [29], and Avrami’s model [21,30,31]. Kinefuchi et al. [30] found that Avrami’s fractional-order kinetic model could describe the desorption process well. Considering the relative merits of each model, Avrami’s model was chosen in this work.

Lopes et al. [32] proposed Avrami’s fractional-order model based on Avrami’s kinetic model to simulate the phase transition and crystal growth of materials. Serna-Guerrero et al. [21] and Liu et al. [33] used this model to study the adsorption process of CO<sub>2</sub> onto amine-based adsorbents. This model can be described as Equation (6):

$$\frac{\partial q_t}{\partial t} = k_A^{n_A} t^{n_A-1} (q_e - q_t) \quad (6)$$

Here,  $k_A$  is the Avrami kinetic constant,  $n_A$  is the Avrami exponent. It reflects that the adsorption mechanisms are changed during the process. The integrated form of the model is described as Equation (7):

$$q_t = q_e (1 - e^{-(k_A t)^{n_A}}) \quad (7)$$

In order to study the desorption process, the model is changed to Equation (8):

$$y = 1 - e^{-(k_A t)^{n_A}} \quad (8)$$

The Avrami model is a reasonable assumption for both chemical adsorption and physical adsorption. The physical desorption of CO<sub>2</sub> is the process of escaping from the fixed number of sites. The chemical desorption of CO<sub>2</sub> is the decomposition of carbamate/bicarbonate [34]. In the implementation of the model, the main challenge is to distinguish between the contributions of chemical adsorption and physical adsorption in the overall CO<sub>2</sub> working capacity measured.

Liu et al. [33] obtained the  $n_A$  of the desorption process in the range of 0.768–0.935 and assumed it is associated with the desorption of physical desorption first and then chemical desorption. However, physical desorption and chemical desorption are concurrent. Serna-Guerrero et al. [35] proposed a new method to identify the contributions of chemical adsorption and physical adsorption in the overall CO<sub>2</sub> adsorption process. Here, the method was applied in the desorption process. As long as

capillary condensation does not occur and the inner surface of the material is freely accessible, physical desorption can be considered proportional to the surface area.

Under such assumptions, the amount of CO<sub>2</sub> physically desorbed on the surface of the modified adsorbent is related to the CO<sub>2</sub> desorption by the unmodified silica support under the same pressure and temperature conditions according to Equation (9):

$$q_{phys(t)} = q_{support} \times \frac{s}{s_{support}} \quad (9)$$

Figure 2 illustrates the desorption proportion of physical desorption and chemical desorption, which can be obtained by Equation (9). Avrami's model was used to fit the curves.

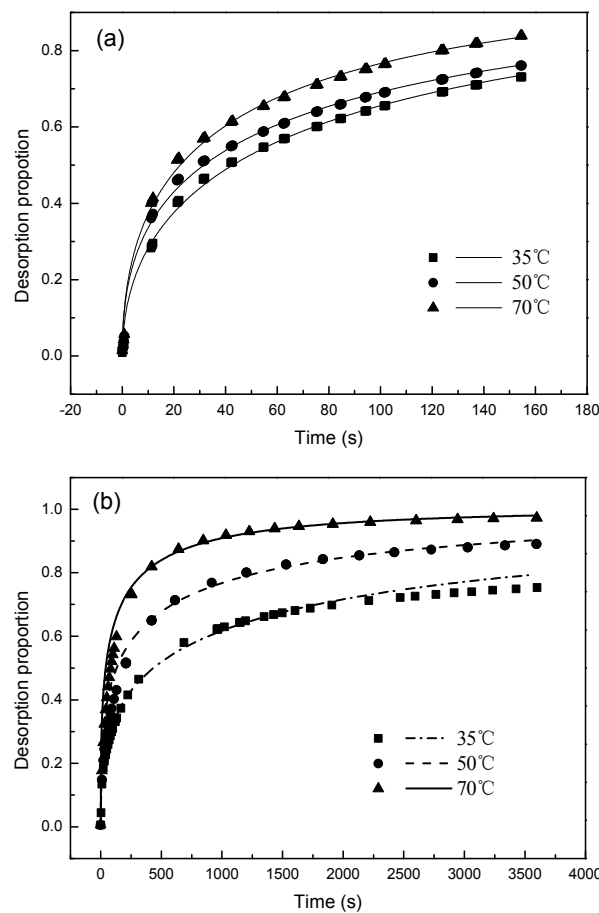


**Figure 2.** Desorption curves of proportion. (a) Physical desorption; (b) chemical desorption.

The temperature dependence of kinetic constant  $k_A$  can be described by the Arrhenius equation:

$$k_A = A e^{-(E_a/RT)} \quad (10)$$

where  $A$  is the Arrhenius pre-exponential factor,  $E_a$  is activation energy,  $R$  is ideal gas constant, and  $T$  is absolute temperature.

The  $\ln k_A$  vs.  $1000/T$  plot for CO<sub>2</sub> desorption based on the values of  $k_A$  according to Equation (10) is presented in Figure 3 and the parameters of the Arrhenius equation are presented in Table 2.

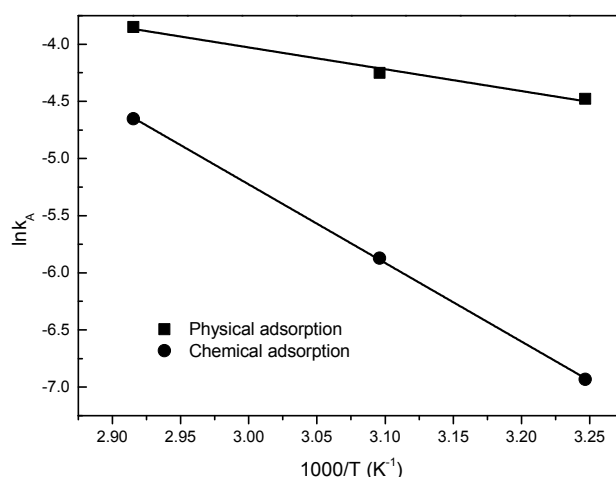


Figure 3. Arrhenius plots for the kinetic parameters.

Table 2. Kinetic parameters for TEPA-based MCM-41 at different temperatures and calculated from CO<sub>2</sub> desorption isotherms fitted to the Arrhenius equation.

Parameters	Physical Desorption			Chemical Desorption		
	35 °C	50 °C	70 °C	35 °C	50 °C	70 °C
$k_A$	0.011	0.014	0.021	$9.04 \times 10^{-4}$	0.00282	0.00954
$n_A$	0.507	0.459	0.495	0.391	0.366	0.388
$R^2$	0.995	0.993	0.994	0.993	0.983	0.984
Parameters of Arrhenius Equation			Desorption Enthalpy $\Delta H$ (kJ/mol)			
$A$ (s <sup>-1</sup> )	5.4517	$4.85 \times 10^6$		MCM-41	MCM-41-TEPA	
$E_a$ (kJ/mol)	15.864	57.152		25.42	70.56	
$R^2$	0.9768	0.9997				

The Avramikinetik parameter  $k_A$  increases with the temperature, suggesting a faster desorption rate under higher temperatures. The mass transfer coefficient increase and the CO<sub>2</sub> desorption curves are steeper with respect to temperature in this work. The values of  $n_A$  for the desorption process are in the range of 0.459–0.507 for physical desorption and 0.366–0.391 for chemical desorption. Liu et al. [33] also obtained the  $n_A$  of the desorption process in the range of 0.768–0.935. The  $E_a$  values are 15.86 kJ/mol and 57.15 kJ/mol for CO<sub>2</sub> physical desorption and chemical desorption, respectively. The whole activation energy is 73.02 kJ/mol, in accordance with the result obtained by thermogravimetric analysis (70.56 kJ/mol) as presented in Table 2. The values obtained here are larger than the values obtained by Liu et al. [27], but smaller than the values calculated by Sun et al. [28]. However, the actual rate-limiting step for CO<sub>2</sub> adsorption could not be obtained by Avrami's model, which needs further investigation.

### 3.3. Desorption Mechanisms

Avrami's model does not provide information concerning the actual rate-limiting steps and diffusion mechanism, since all adsorption steps are lumped together. According to the literature [36,37], there are five main mechanisms of mass transfer during desorption: (a) surface reaction, which occurs via physical or chemical interaction on desorption sites; (b) inner particle diffusion; (c) intraparticle diffusion (pore diffusion); (d) film diffusion; and (e) external diffusion. The overall rate of the desorption process may be controlled by any of these mechanisms or by a combination of two steps, in some cases. Based on the established fact that the (a), (b), and (e) steps are relatively fast, it is assumed that desorption kinetic process is controlled by CO<sub>2</sub> film diffusion or intraparticle diffusion. Therefore, in order to better understand the rate-limiting step for CO<sub>2</sub> desorption kinetics on

amine-based MCM-41, the kinetic data was analyzed by the intraparticle diffusion model and Boyd's film diffusion model.

#### (i) Intraparticle Diffusion Model

During the desorption mechanism, the CO<sub>2</sub> molecules interact not only with the outer surface, but also diffuse out the mesopores and desorbed from the inner surface. The pore-diffusion process influences the adsorption rate and becomes the rate-limiting step.

Weber and Morris [38] proposed that if the adsorption process is influenced by intraparticle diffusion, the adsorption capacity ( $q_t$ ) varies linearly with the square root of time [20,36]. This model is derived from Fick's second law of diffusion with the assumptions below:

- (a) The external resistance of mass transfer is only significant at the beginning of diffusion.
- (b) The diffusion direction is radial.
- (c) The pore diffusivity is constant.

The model is an approximation of pore diffusion kinetics and could identify the desorption mechanism, which is expressed in Equation (11):

$$q_t = k_d t^{0.5} + C \quad (11)$$

In Equation (11),  $k_d$  is the intraparticle diffusion rate constant, and its value can be evaluated from the slope of plot of  $q_t$  versus  $t^{0.5}$ , and  $C$  is the intercept associating with the thickness of boundary layer [20]. Usually, the intraparticle diffusion model includes three steps. The first one is intraparticle diffusion; the second is the external diffusion adsorption or boundary layer diffusion; and the third one is the final equilibrium stage.

According to this model, if intraparticle diffusion is the sole rate-limiting step, the plot is linear and should pass through the origin ( $C = 0$ ). Otherwise, other processes may control the adsorption rate.

As seen in Figure 3, the Weber–Morris plots for CO<sub>2</sub> adsorption on MCM-41 at 35, 50, and 70 °C are not linear and exhibit trilinearity, suggesting the existence of three steps for MCM-41. The first region is correlated to gradual desorption stage, where intraparticle diffusion play an important role. The second portion describes the diffusion of CO<sub>2</sub> through the external surface of MCM-41 to the bulk gas phase and it is attributed to the boundary layer diffusion of CO<sub>2</sub>. The last stage is the final equilibrium region.

The linear plots corresponding to the first stage pass through the origin, indicating that the pore-diffusion is the only rate-limiting step. However, the linear plots of the second portion indicate the boundary layer effect over the adsorption of CO<sub>2</sub>. It is worth to note the fact that at 70 °C, the intercept of the plot is closer to the origin compared with the values of 35 and 50 °C. A possible explanation is that with the increase of temperature, the film is weaker and therefore the rate of film diffusion increases. It is reasonable to predict that under higher temperature, intraparticle diffusion is the sole rate-limiting factor for the overall CO<sub>2</sub> adsorption process. However, under lower temperature, both pore diffusion and film diffusion contribute to the CO<sub>2</sub> desorption kinetics on MCM-41.

Figure 4b shows the Weber–Morris plots of MCM-41-TEPA. The whole range can be divided into four regions, and it reveals that there are four successive steps for CO<sub>2</sub> desorption on MCM-41-TEPA.

In the first stage of 0–0.7, the plots pass through the origin, the rate limiting step is intraparticle diffusion, CO<sub>2</sub> adsorbed through physical adsorption is easier to be desorbed in this stage. The second region is correlated to a gradual desorption stage, where the decomposition of carbamate/bicarbonate and intraparticle diffusion control the rate, under higher temperature, the chemical reaction is easier to process, so the intercept of the plot under 70 °C is closer to the origin compared with 35 and 50 °C. The third portion describes the diffusion of CO<sub>2</sub> through the external surface to the bulk gas phase, and this stage is correlated to the boundary layer diffusion of CO<sub>2</sub>. For MCM-41-TEPA under 70 °C, this portion is very short. The last stage is the final equilibrium region. It is assumed that for MCM-41-TEPA, surface reaction is also a rate-limiting element.

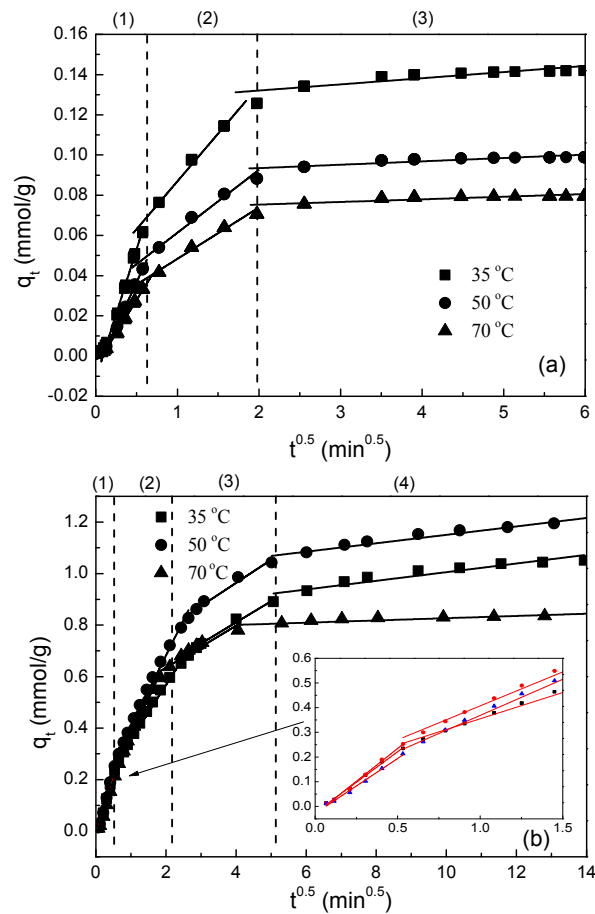


**Figure 4.** Plots of Weber–Morris intraparticle diffusion model for CO<sub>2</sub> adsorption on (a) mesoporous MCM-41 and (b) MCM-41-TEPA at 35, 50, and 70 °C.

#### (ii) Boyd Kinetic Film-Diffusion Model

Boyd kinetic film-diffusion model was used to analyze the real rate-limiting step. This model assumes that the main diffusion resistance is the boundary layer surrounding the adsorbent particle. The model is expressed as Equation (12):

$$F = 1 - \frac{6}{\pi^2 \sum_{n=1}^{\infty} \frac{1}{n^2} \exp(-n^2 B_t)} \quad (12)$$

where  $F$  is the fractional adsorbed amount at different time  $t$ , as calculated using Equation (13):

$$F = \frac{q_t}{q_e} \quad (13)$$

$B_t$  can be calculated as [39]:

For  $F > 0.85$ ,

$$B_t = 0.4977 - \ln(1 - F) \quad (14)$$

For  $F < 0.85$ ,

$$B_t = \left( \sqrt{\pi} - \sqrt{\pi - \left( \frac{\pi^2 F}{3} \right)} \right)^2 \quad (15)$$

The equations are used to predict whether the desorption rate takes place through particle diffusion or film diffusion mechanism. If the plot of  $B_t$  versus  $t$  is linear and passes through the origin, the film diffusion gives minimal function, and pore diffusion controls the mass transfer rate. However, when the plot is not linear, or linear but not pass through the origin, film diffusion or chemical reaction makes the maximum contribution to the desorption rate [40,41].

Mass transfer mechanism can be explored in the analysis of data from Boyd's model. As can be seen in Figure 5a, for MCM-41, porediffusion becomes more important at higher temperatures, since the intercepts of 70 °C approach zero in comparison with 35 and 50 °C. This is in accordance with the results obtained by the intraparticle diffusion model. However, for MCM-41-TEPA, the desorption mechanisms become very complicated. It is very difficult to distinguish the influence of surface reaction and diffusion at the gas/solid interface in batch systems. A mix of surface reaction and diffusion models will be used in the future work to explore further the desorption mechanism of amine modified materials.

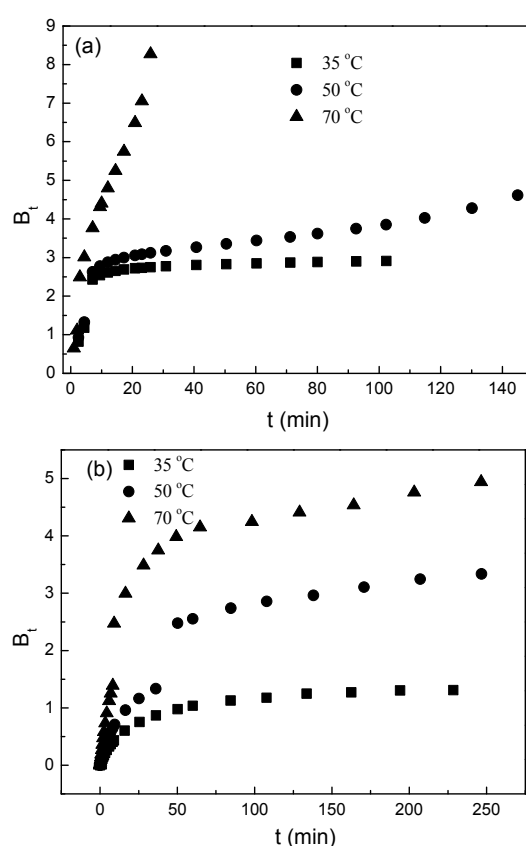


**Figure 5.** Boyd plots for CO<sub>2</sub> desorption from MCM-41 (a) and MCM-41-TEPA and (b) at 35, 50, and 70 °C.

#### 4. Conclusions

In this work, ZLC is used to study the desorption kinetics and desorption mechanisms, which are important to evaluate the energy requirements for regeneration of CO<sub>2</sub> and to design the CO<sub>2</sub> capture reactors. A novel method is presented to identify the portion of chemical adsorption and physical adsorption, which is beneficial for kinetic analysis of CO<sub>2</sub> adsorption on amine-based mesoporous materials at different temperatures. The physical adsorption and chemical adsorption of CO<sub>2</sub> on MCM-41-TEPA are successfully described using Avrami's model. The value of  $E_a$  is calculated as 15.86 kJ/mol and 57.15 kJ/mol for CO<sub>2</sub> physical desorption and chemical desorption, respectively. The whole activation energy for MCM-41 is 73.02 kJ/mol.

For MCM-41, both intraparticle diffusion model and Boyd's model indicate that pore-diffusion becomes predominate at higher temperature. However, for MCM-41-TEPA, the desorption mechanisms become complicated due to the chemical reaction. It is difficult to distinguish the influence of surface reaction and diffusion at the gas/solid interface in batch systems. As for MCM-41-TEPA, the desorption process contains four rate-limiting steps, including surface reaction, compared with pure MCM-41 besides surface reaction.

**Acknowledgments:** Authors gratefully acknowledge National Natural Science Foundation of China (91434120) and Major Special Project of Shanxi Province (MD2014-03, MD2015-01).

**Author Contributions:** Yang Teng designed the experiments, analyzed the data and wrote the paper; Zhilin Liu performed the experiments; Kai Zhang and Gang Xu analyzed the data and provided the helpful discussion.

**Conflicts of Interest:** The authors declare no conflict of interest.

## Abbreviations

The following abbreviations are used in this manuscript:

TEPA	Tetraethylenepentamine
CCS	CO <sub>2</sub> capture and sequestration
ZLC	Zero-Length Column
XRD	X-ray diffraction
MS	mass spectrometer

## References

1. Tan, Y.; Nookuea, W.; Li, H.; Rhorin, E.; Yan, J. Property impacts on carbon capture and storage (CCS) processed: A review. *Energy Convers. Manag.* **2016**, *118*, 204–222. [[CrossRef](#)]
2. Serna-Guerrero, R.; Belmabkhout, Y.; Sayari, A. Further investigations of CO<sub>2</sub> capture using triamine-grafted pore-expanded mesoporous silica. *Chem. Eng. J.* **2010**, *158*, 513–519. [[CrossRef](#)]
3. Bollini, P.; Didas, S.A.; Jones, C.W. Amine-oxide hybrid materials for acid gas separations. *J. Mater. Chem.* **2011**, *21*, 15100–15120. [[CrossRef](#)]
4. Loganathan, S.; Ghoshal, A.K. Amine tethered pore-expanded MCM-41: A promising adsorbent for CO<sub>2</sub> capture. *Chem. Eng. J.* **2017**, *308*, 817–839. [[CrossRef](#)]
5. Chen, C.; Bhattacharjee, S. Trimodal nanoporous silica as a support for amine-based CO<sub>2</sub> adsorbents: Improvement in adsorption capacity and kinetics. *Appl. Surf. Sci.* **2017**, *396*, 1515–1519. [[CrossRef](#)]
6. Xu, X.; Song, C.; Andersen, J.M.; Mille, B.G.; Scaroni, A.W. Novel polyethylenimine-modified mesoporous molecular sieve of MCM-41 type as high-capacity adsorbent for CO<sub>2</sub> capture. *Energy Fuels* **2002**, *16*, 1463–1469. [[CrossRef](#)]
7. Bezerra, D.P.; Oliveira, R.S.; Vieira, R.S.; Cavalcante, C.L.; Azevedo, D.C.S. Adsorption of CO<sub>2</sub> on nitrogen-enriched activated carbon and zeolite 13X. *Adsorpt. J. Int. Adsorpt. Soc.* **2011**, *17*, 235–246. [[CrossRef](#)]
8. Liu, Z.; Teng, Y.; Zhang, K.; Chen, H.; Yang, Y. CO<sub>2</sub> adsorption performance of different amine-based siliceous MCM-41 materials. *J. Energy Chem.* **2015**, *24*, 322–330. [[CrossRef](#)]
9. Qi, G.; Wang, Y.; Estevez, L.; Duan, X.; Anako, N.; Park, A.-H.A.; Li, W.; Jones, C.W.; Giannelis, E.P. High efficiency nanocomposite sorbents for CO<sub>2</sub> capture based on amine-functionalized mesoporous capsules. *Energy Environ. Sci.* **2011**, *4*, 444–452. [[CrossRef](#)]
10. Sanz, R.; Calleja, G.; Arencibia, A.; Sanz-Pérez, E.S. CO<sub>2</sub> capture with pore-expanded MCM-41 silica modified by double functionalization. *Microporous Mesoporous Mater.* **2015**, *209*, 167–171. [[CrossRef](#)]
11. Vaidhyanathan, R.; Iremonger, S.S.; Dawson, K.W.; Shimizu, G.K.H. An amine-functionalized metal organic framework for preferential CO<sub>2</sub> adsorption at low pressures. *Chem. Commun.* **2009**, 5230–5232. [[CrossRef](#)] [[PubMed](#)]
12. Eic, M.; Ruthven, D.M. A new experimental-technique for measurement of intracrystalline diffusivity. *Zeolites* **1988**, *8*, 40–45. [[CrossRef](#)]
13. Cavalcante, C.L., Jr.; Ruthven, D.M. Adsorption of Branched and Cyclic Paraffins in Silicalite. 1. Equilibrium. *Ind. Eng. Chem. Res.* **1995**, *34*, 177–184. [[CrossRef](#)]
14. Friedrich, D.; Mangano, E.; Brandani, S. Automatic estimation of kinetic and isotherm parameters from ZLC experiments. *Chem. Eng. Sci.* **2015**, *126*, 616–624. [[CrossRef](#)]

15. Hu, X.Y.; Mangano, E.; Friedrich, D.; Ahn, H.; Brandani, S. Diffusion mechanism of CO<sub>2</sub> in 13X zeolite beads. *Adsorption* **2014**, *20*, 121–135. [[CrossRef](#)]
16. Martín-Martínez, J.M.; Torregrosa-Maciá, R.; Mittelmeijer-Hazeleger, M.C. Mechanisms of adsorption of CO<sub>2</sub> in the micropores of activated anthracite. *Fuel* **1995**, *74*, 111–114. [[CrossRef](#)]
17. Bacsik, Z.; Ahlsten, N.; Ziadi, A.; Zhao, G.; Garcia-Bennett, A.E.; Martín-Matute, B.; Hedin, N. Mechanisms and kinetics for sorption of CO<sub>2</sub> on bicontinuous mesoporous silica modified with *n*-propylamine. *Langmuir* **2011**, *27*, 11118–11128. [[CrossRef](#)] [[PubMed](#)]
18. Liu, Z.; Teng, Y.; Zhang, K.; Cao, Y.; Pan, W. CO<sub>2</sub> adsorption properties and thermal stability of different amine-impregnated MCM-41 materials. *J. Fuel Chem. Technol.* **2013**, *41*, 469–475. [[CrossRef](#)]
19. Brandani, S.; Ruthven, D.M. Moments analysis of the Zero Length Column method. *Ind. Eng. Chem. Res.* **1996**, *35*, 315–319. [[CrossRef](#)]
20. Yousef, R.I.; El-Eswed, B.; Al-Muhtaseb, A.H. Adsorption characteristics of natural zeolites as solid adsorbents for phenol removal from aqueous solutions: Kinetics, mechanism, and thermodynamics studies. *Chem. Eng. J.* **2011**, *171*, 1143–1149. [[CrossRef](#)]
21. Serna-Guerrero, R.; Sayari, A. Modeling adsorption of CO<sub>2</sub> on amine-functionalized mesoporous silica. 2: Kinetics and breakthrough curves. *Chem. Eng. J.* **2010**, *161*, 182–190. [[CrossRef](#)]
22. Liu, F.Q.; Wang, L.; Huang, Z.G.; Li, C.Q.; Li, W.; Li, R.X.; Li, W.H. Amine-rethered adsorbents based on three-dimensional macroporous silica for CO<sub>2</sub> capture from simulated flue gas and air. *ACS Appl. Mater. Interfaces* **2014**, *6*, 4371–4381. [[CrossRef](#)] [[PubMed](#)]
23. Lin, Y.; Yan, Q.; Kong, C.; Chen, L. Polyethyleneimine incorporated metal-organic frameworks adsorbent for highly selective CO<sub>2</sub> capture. *Sci. Rep.* **2013**, *3*, 1859. [[CrossRef](#)] [[PubMed](#)]
24. Dzubak, A.L.; Lin, L.-C.; Kim, J.; Swisher, J.A.; Poloni, R.; Maximoff, S.N.; Smit, B.; Gagliardi, L. Ab initio carbon capture in open-site metal-organic frameworks. *Nat. Chem.* **2012**, *4*, 810–816. [[CrossRef](#)] [[PubMed](#)]
25. Wurzbacher, J.A.; Gebald, C.; Steinfeld, A. Separation of CO<sub>2</sub> from air by temperature-vacuum swing adsorption using diamine-functionalized silica gel. *Energy Environ. Sci.* **2011**, *4*, 3584–3592. [[CrossRef](#)]
26. Jeppu, G.P.; Clement, T.P. A modified Langmuir-Freundlich isotherm model for simulating pH-dependent adsorption effects. *J. Contam. Hydrol.* **2012**, *129–130*, 46–53. [[CrossRef](#)] [[PubMed](#)]
27. Gargiulo, N.; Peluso, A.; Aprea, P.; Pepe, F.; Caputo, D. CO<sub>2</sub> Adsorption on polyethylenimine-functionalized SBA-15 mesoporous silica: Isotherms and modeling. *J. Chem. Eng. Data* **2014**, *59*, 896–902. [[CrossRef](#)]
28. Haerifar, M.; Azizian, S. Mixed surface reaction and diffusion-controlled kinetic model for adsorption at the solid/solution interface. *J. Phys. Chem. C* **2013**, *117*, 8310–8317. [[CrossRef](#)]
29. Wang, Y.X.; Liu, B.S.; Zheng, C. Preparation and adsorption properties of corncob-derived activated carbon with high surface area. *J. Chem. Eng. Data* **2010**, *55*, 4669–4676. [[CrossRef](#)]
30. Kinefuchi, I.; Yamaguchi, H.; Sakiyama, Y.; Takagi, S.; Matsumoto, Y. Inhomogeneous decomposition of ultrathin oxide films on Si(100): Application of Avrami kinetics to thermal desorption spectra. *J. Chem. Phys.* **2008**, *128*, 164712. [[CrossRef](#)] [[PubMed](#)]
31. Moura, K.O.; Pastore, H.O. Comparative adsorption of CO<sub>2</sub> by mono-, di-, and triamino-organofunctionalized magnesium phyllosilicates. *Environ. Sci. Technol.* **2013**, *47*, 12201–12210. [[CrossRef](#)] [[PubMed](#)]
32. Lopes, E.C.N.; dos Anjos, F.S.C.; Vieira, E.F.S.; Cestari, A.R. An alternative Avrami equation to evaluate kinetic parameters of the interaction of Hg(II) with thin chitosan membranes. *J. Colloid Interface Sci.* **2003**, *263*, 542–547. [[CrossRef](#)]
33. Liu, Q.; Shi, J.; Zheng, S.; Tao, M.; He, Y.; Shi, Y. Kinetics studies of CO<sub>2</sub> adsorption/desorption on amine-functionalized multiwalled carbon nanotubes. *Ind. Eng. Chem. Res.* **2014**, *53*, 11677–11683. [[CrossRef](#)]
34. Sun, Z.; Fan, M.; Argyle, M. Desorption kinetics of the monoethanolamine/macroporous TiO<sub>2</sub>-based CO<sub>2</sub> separation process. *Energy Fuels* **2011**, *25*, 2988–2996. [[CrossRef](#)]
35. Serna-Guerrero, R.; Belmabkhout, Y.; Sayari, A. Modeling CO<sub>2</sub> adsorption on amine-functionalized mesoporous silica: 1. A semi-empirical equilibrium model. *Chem. Eng. J.* **2010**, *161*, 173–181. [[CrossRef](#)]
36. Loganathan, S.; Tikmani, M.; Edubilli, S.; Mishra, A.; Ghoshal, A.K. CO<sub>2</sub> adsorption kinetics on mesoporous silica under wide range of pressure and temperature. *Chem. Eng. J.* **2014**, *256*, 1–8. [[CrossRef](#)]
37. Rudzinski, W.; Plazinski, W. Theoretical description of the kinetics of solute adsorption at heterogeneous solid/solution interfaces: On the possibility of distinguishing between the diffusional and the surface reaction kinetics models. *Appl. Surf. Sci.* **2007**, *253*, 5827–5840. [[CrossRef](#)]
38. Weber, W.J.; Morris, J.C. Kinetics of adsorption on carbon from solution. *J. Sanit. Eng. Div.* **1963**, *89*, 31–60.

39. Reichenberg, D. Properties of ion-exchange resins in relation to their structure. III. Kinetics of exchange. *J. Am. Chem. Soc.* **1953**, *75*, 589–597. [[CrossRef](#)]
40. Hameed, B.H.; Tan, I.A.W.; Ahmad, A.L. Adsorption isotherm, kinetic modeling and mechanism of 2,4,6-trichlorophenol on coconut husk-based activated carbon. *Chem. Eng. J.* **2008**, *144*, 235–244. [[CrossRef](#)]
41. Sharma, P.; Das, M.R. Removal of a cationic dye from aqueous solution using grapheme oxide nanosheets: Investigation of adsorption parameters. *J. Chem. Eng. Data* **2013**, *58*, 151–158. [[CrossRef](#)]



© 2017 by the authors; licensee MDPI, Basel, Switzerland. This article is an open access article distributed under the terms and conditions of the Creative Commons Attribution (CC-BY) license (<http://creativecommons.org/licenses/by/4.0/>).